Visible light communication using InGaN optical sources with AlInGaP nanomembrane down-converters

J. M. M. Santos,[1, *] S. Rajbhandari,[2] D. Tsonev,[3] H. Chun,[2] B. Guilhabert,[1] A. B. Krysa,[4] A. E. Kelly,[5] H. Haas,[3] D. C. O'Brien,[2] N. Laurand[1] and M. D. Dawson[1]

[1]*Institute of Photonics, Department of Physics, SUPA, University of Strathclyde, Glasgow, UK*
[2]*Department of Engineering Science, University of Oxford, Oxford, UK*
[3]*Li-Fi R&D Centre, Institute for Digital Communications, University of Edinburgh, Edinburgh, UK*
[4]*Electronic & Electrical Engineering, University of Sheffield, Sheffield, UK*
[5]*Electronic & Electrical Engineering, University of Glasgow, Glasgow, UK*
[*]*joao.santos@strath.ac.uk*

Abstract: We report free space visible light communication using InGaN sources, namely micro-LEDs and a laser diode, down-converted by a red-emitting AlInGaP multi-quantum-well nanomembrane. In the case of micro-LEDs, the AlInGaP nanomembrane is capillary-bonded between the sapphire window of a micro-LED array and a hemispherical sapphire lens to provide an integrated optical source. The sapphire lens improves the extraction efficiency of the color-converted light. For the case of the down-converted laser diode, one side of the nanomembrane is bonded to a sapphire lens and the other side optionally onto a dielectric mirror; this nanomembrane-lens structure is remotely excited by the laser diode. Data transmission up to 870 Mb/s using pulse amplitude modulation (PAM) with fractionally spaced decision feedback equalizer is demonstrated for the micro-LED-integrated nanomembrane. A data rate of 1.2 Gb/s is achieved using orthogonal frequency division multiplexing (ODFM) with the laser diode pumped sample.

OCIS codes: (230.0250) Optoelectronics; (230.3670) Light-emitting diodes; (250.5590) Quantum-well, -wire and -dot devices; (060.4510) Optical communications; (060.2630) Frequency modulation; (060.2605) Free-space optical communication.

References and links

1. J. J. Wierer, Jr., J. Y. Tsao, and D. S. Sizov, "Comparison between blue lasers and light-emitting diodes for future solid-state lighting," Laser Photonics Rev. **993**(6), 963–993 (2013).
2. C. W. Chow, C. H. Yeh, Y. Liu, and Y. F. Liu, "Digital signal processing for light emitting diode based visible light communication," IEEE Photonics Soc. Newletter **26**(5), 9–13 (2012).
3. L. Grobe, A. Paraskevopoulos, J. Hilt, D. Schulz, F. Lassak, F. Hartlieb, C. Kottke, V. Jungnickel, and K.-D. Langer, "High-speed visible light communication systems," IEEE Commun. Mag. **51**(12), 60–66 (2013).
4. M. R. Krames, O. B. Shchekin, R. Müller-Mach, G. O. Müller, L. Zhou, G. Harbers, and M. G. Craford, "Status and future of high-power light-emitting diodes for solid-state lighting," J. Disp. Technol. **3**(2), 160–175 (2007).
5. M. S. Shur and A. Žukauskas, "Solid-state lighting: toward superior illumination," Proc. IEEE **93**(10), 1691–1703 (2005).
6. J. Herrnsdorf, B. Guilhabert, J. J. D. McKendry, Z. Gong, D. Massoubre, S. Zhang, S. Watson, A. E. Kelly, E. Gu, N. Laurand, and M. D. Dawson, "Hybrid organic/GaN photonic crystal light-emitting diode," Appl. Phys. Lett. **101**(14), 141122 (2012).
7. M. T. Sajjad, P. P. Manousiadis, H. Chun, D. A. Vithanage, S. Rajbhandari, A. L. Kanibolotsky, G. Faulkner, D. O'Brien, P. J. Skabara, I. D. W. Samuel, and G. A. Turnbull, "Novel fast color-converter for visible light communication using a blend of conjugated polymers," ACS Photonics **2**(2), 194–199 (2015).
8. N. Laurand, B. Guilhabert, J. McKendry, A. E. Kelly, B. Rae, D. Massoubre, Z. Gong, E. Gu, R. Henderson, and M. D. Dawson, "Colloidal quantum dot nanocomposites for visible wavelength conversion of modulated optical signals," Opt. Mater. Express **2**(3), 250–260 (2012).
9. J. M. M. Santos, B. E. Jones, P. J. Schlosser, S. Watson, J. Herrnsdorf, B. Guilhabert, J. J. D. McKendry, J. De

Jesus, T. A. Garcia, M. C. Tamargo, A. E. Kelly, J. E. Hastie, N. Laurand, and M. D. Dawson, "Hybrid GaN LED with capillary-bonded II–VI MQW color-converting membrane for visible light communications," Semicond. Sci. Technol. **30**(3), 035012 (2015).

10. D. Schiavon, M. Binder, A. Loeffler, and M. Peter, "Optically pumped GaInN / GaN multiple quantum wells for the realization of efficient green light-emitting devices optically pumped GaInN / GaN multiple quantum wells for the realization of efficient green light-emitting devices," Appl. Phys. Lett. **102**(11), 113509 (2013).

11. M. A. Haase, J. Xie, T. A. Ballen, J. Zhang, B. Hao, Z. H. Yang, T. J. Miller, X. Sun, T. L. Smith, and C. A. Leatherdale, "II–VI semiconductor color converters for efficient green, yellow, and red light emitting diodes," Appl. Phys. Lett. **96**(23), 231116 (2010).

12. J. J. D. McKendry, R. P. Green, A. E. Kelly, Z. Gong, B. Guilhabert, D. Massoubre, E. Gu, and M. D. Dawson, "High-speed visible light communications using individual pixels in a micro light-emitting diode array," IEEE Photonics Technol. Lett. **22**(18), 1346–1348 (2010).

13. Z. L. Liau, "Semiconductor wafer bonding via liquid capillarity," Appl. Phys. Lett. **77**(5), 651 (2000).

14. Z. Gong, S. Jin, Y. Chen, J. McKendry, D. Massoubre, I. M. Watson, E. Gu, and M. D. Dawson, "Size-dependent light output, spectral shift, and self-heating of 400 nm InGaN light-emitting diodes," J. Appl. Phys. **107**(1), 013103 (2010).

15. D. O'Brien, R. Turnbull, H. Le Minh, G. Faulkner, O. Bouchet, P. Porcon, M. El Tabach, E. Gueutier, M. Wolf, L. Grobe, and J. Li, "High-speed optical wireless demonstrators: conclusions and future directions," J. Lightwave Technol. **30**(13), 2181–2187 (2012).

16. D. Tsonev, H. Chun, S. Rajbhandari, J. J. D. Mckendry, S. Videv, E. Gu, M. Haji, S. Watson, A. E. Kelly, G. Faulkner, M. D. Dawson, H. Haas, and D. O. Brien, "A 3-Gb/s single-LED OFDM-based wireless VLC link using a gallium nitride μLED," IEEE Photonics Soc. Newletter **26**(7), 637–640 (2014).

17. Y. C. Shen, G. O. Mueller, S. Watanabe, N. F. Gardner, A. Munkholm, and M. R. Krames, "Auger recombination in InGaN measured by photoluminescence," Appl. Phys. Lett. **91**(14), 141101 (2007).

18. J. Hader, J. V. Moloney, B. Pasenow, S. W. Koch, M. Sabathil, N. Linder, and S. Lutgen, "On the importance of radiative and Auger losses in GaN-based quantum wells," Appl. Phys. Lett. **92**(26), 261103 (2008).

19. E. F. Schubert, *Light-Emitting Diodes*, 2nd ed. (Cambridge University, 2006).

20. C. Y. Liu, S. Yuan, J. R. Dong, and S. J. Chua, "Temperature dependence of photoluminescence intensity from AlGaInP/GaInP multi-quantum well laser structures," J. Cryst. Growth **268**(3-4), 426–431 (2004).

21. R. P. Green, J. J. D. McKendry, D. Massoubre, E. Gu, M. D. Dawson, and A. E. Kelly, "Modulation bandwidth studies of recombination processes in blue and green InGaN quantum well micro-light-emitting diodes," Appl. Phys. Lett. **102**(9), 091103 (2013).

22. J. Grubor, S. Randel, K. D. Langer, and J. W. Walewski, "Broadband information broadcasting using LED-based interior lighting," J. Lightwave Technol. **26**(24), 3883–3892 (2008).

23. S. Watson, M. Tan, S. P. Najda, P. Perlin, M. Leszczynski, G. Targowski, S. Grzanka, and A. E. Kelly, "Visible light communications using a directly modulated 422 nm GaN laser diode," Opt. Lett. **38**(19), 3792–3794 (2013).

24. C. Lee, C. Zhang, M. Cantore, R. M. Farrell, S. H. Oh, T. Margalith, J. S. Speck, S. Nakamura, J. E. Bowers, and S. P. DenBaars, "4 Gbps direct modulation of 450 nm GaN laser for high-speed visible light communication," Opt. Express **23**(12), 16232–16237 (2015).

25. S. Randel, F. Breyer, S. C. J. Lee, and J. W. Walewski, "Advanced modulation schemes for short-range optical communications," IEEE J. Sel. Top. Quantum Electron. **16**(5), 1280–1289 (2010).

26. S. Loquai, R. Kruglov, B. Schmauss, C. Bunge, F. Winkler, O. Ziemann, E. Hartl, and T. Kupfer, "Comparison of modulation schemes for 10. 7 Gb/s transmission over large-core 1 mm PMMA polymer optical fiber," J. Lightwave Technol. **31**(13), 2170–2176 (2013).

1. Introduction

Solid-state visible light sources based on the AlInGaN material systems have become key enablers for a number of applications including lighting and illumination, displays, and consumer electronics. For example, InGaN-based white-light emitting diodes are replacing older light bulb technologies for home and street illuminations while InGaN laser diodes are used for optical data storage and are being considered for future ultra-efficient lighting [1]. An emerging application for InGaN-based white LEDs is visible light communications (VLC), which has been gathering a lot of attention recently [2,3]. Because practical InGaN optoelectronic sources do not yet cover the entire visible spectrum (the device efficiency drops continuously for wavelengths above 500 nm [4]), a blue-emitting GaN source often needs to be combined with color-converting materials to access longer wavelengths, or generate white light. This is usually done with rare-earth phosphors, as in commercial white LEDs [5]. However, phosphors respond slowly to modulated light, which is not ideal for VLC. Other color-converting materials are therefore being researched for VLC including organic semiconductors [6,7], colloidal nanocrystals [8] and inorganic semiconductor

epilayers [9]. The latter offers an all-inorganic, photostable solution to color-conversion, which is particularly attractive for high power applications.

Recently, we have demonstrated a hybrid green-emitting LED based on a II-VI multi-quantum well (MQW) epilayer structure a couple of micron-thick for color-conversion of a blue micro-LED [9]. Other groups had previously shown similar heterogeneous hybridization of epitaxial structures as a way to push the emission of GaN LEDs to longer wavelengths [10,11]. In this work, we report the implementation of a red-emitting AlInGaP semiconductor color-converting structure and demonstrate free space VLC when it is combined with blue InGaN sources. The AlInGaP structure is a nanomembrane (NM) with a thickness below 400 nm and comprising a multi-quantum well active region. The NM format facilitates the heterogeneous integration of the color-converter with other materials and structures through capillary bonding. We focus on a device implementation where the AlInGaP NM is fully integrated with a GaN micro-LED array. The result is an array of hybrid red LEDs that benefits from the relatively high modulation bandwidth of the underlying blue micro-LEDs [12]. Additionally, we demonstrate a proof-of-principle format for remote pumping with a blue laser diode where the NM is simply bonded onto a hemispherical sapphire lens. In both implementations, VLC experiments are done by modulating the GaN-based source with the modulated blue light being transferred to red by radiative down-conversion through the NM.

The paper is organized as follows: section 2 describes the design of the AlInGaP NM and its integration with the micro-LED array and/or the hemispherical sapphire lens. A description of the micro-LED array and the characterization methods are also given. Sections 3 and 4 report and discuss, respectively, the continuous-wave (CW) characteristics of the NM-based sources, and their dynamic and VLC performance under M-ary pulse amplitude modulation (M-PAM) and orthogonal frequency-division multiplexing (OFDM) modulation schemes.

2. Device fabrication and characterization

2.1 Design and fabrication

The color-converter structure is based on epitaxial AlInGaP grown on GaAs substrate by metalorganic vapor phase epitaxy. The active region is made of 3 pairs of InGaP quantum wells, with AlInGaP as the barrier material, designed for a room temperature photoluminescence emission at 648 nm. The 2λ length of the MQW region (excluding the GaAs buffer) is chosen so that the finalized NM absorbs >90% of excitation light at 450 nm. To obtain the NM, the GaAs substrate is removed by wet etching using a solution of H_3PO_4:H_2O_2:H_2O at a ratio of 3:4:3. The resulting NM has a thickness of <400 nm, and a typical surface area of a few mm^2.

In the first device implementation (hybrid LED), the NM is capillary-bonded using deionized water [13] onto the sapphire window (polished epi-substrate) of the micro-LED chip [Fig. 1(a)]. This technique enables direct Van der Waal's bonding between surfaces without requiring interlayers. A 2mm diameter sapphire hemispherical lens with a refractive index of 1.7 is in turn capillary-bonded on top of the NM to finalize the hybrid device [Fig. 1(b)]. The micro-LED chip, with peak emission at 450 nm, is fabricated using a commercial p-i-n GaN structure grown on c-plane sapphire, following the procedure reported in [14]. The chip is made of 8 micro-LED pixels of 4 different sizes, 50 x 50 μm^2, 75 x 75 μm^2, 100 x 100 μm^2 and 150 x 150 μm^2. It is mounted onto a printed circuit board and wire bonded to metal tracks connected to SMA connectors, in such a way that each pixel from the micro-LED array can be individually addressed. Figure 1(c) presents a photoluminescence spectrum from the NM with a photograph as inset of the hybrid device under current injection with the color-converted light visible in the center.

In the second NM implementation, for the laser diode (LD) pumping embodiment, the NM is simply bonded to a sapphire hemispherical lens as depicted in Fig. 1(d). The other side

of the membrane is optionally placed in contact with a dielectric mirror. The 450nm LD (OSRAM PL450B) pump is mounted in a Peltier-cooled metallic mount kept at a constant temperature of 25°C.
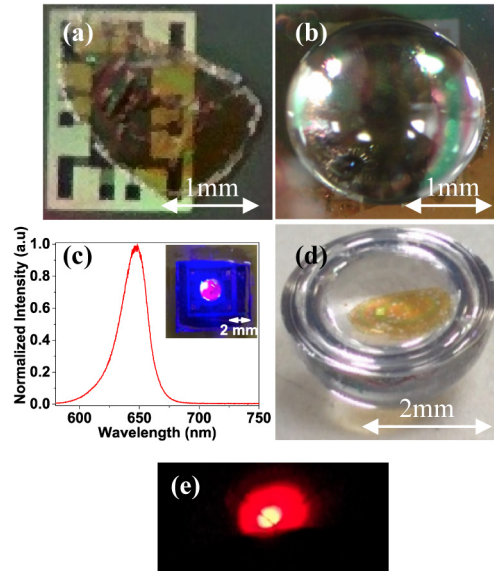

Fig. 1. MQW NM a) capillary bonded onto the sapphire window of the micro-LED chip, b) sandwiched in-between the sapphire hemispherical lens and the micro-LED window, c) spectrum with a picture in inset from the hybrid LED with integrated sapphire lens under operation, d) capillary bonded onto the sapphire hemispherical lens and e) color-converted light, imaged on a screen, from the LD-pumped NM.

2.2 Experimental methods

For reference, the stand-alone blue micro-LEDs as well as the 450nm LD were first characterized, independently of the NM, in terms of optical power, emission spectrum and modulation bandwidths. The same measurements were then done with the AlInGaP NM (integrated with the micro-LEDs or remotely excited for LD pumping).

A set of aspheric lenses with focal length of 32 mm and high numerical aperture (NA of 0.612) were used to collect and focus the emission into a Femto HSA-X-S-1G4-SI photoreceiver (bandwidth of 1.4 GHz). For bandwidth measurements, the micro-LED or LD was simultaneously driven with a dc bias current and a frequency-swept modulated signal ($0.250V_{p-p}$) that were combined through a wideband (0.1–6000 MHz) Bias-Tee. An Agilent HP 8753ES Network Analyzer was used to provide the modulation signal and to record the device frequency response as detected by the photoreceiver. A long-pass filter (550 nm cut-off wavelength) was placed before the receiver for measurements of the down-converted light. The modulation bandwidth was extracted from the detected modulation amplitude versus frequency as detailed in [8,9]. The optical spectra were recorded with an Ocean Optics USB4000 Fiber Optic Spectrometer (2.5 nm resolution).

A similar set-up was used for the VLC demonstrations of section 4, with some specifics described here. For both PAM and OFDM, the modulated signal was generated offline in MATLAB® environment and loaded to an Agilent 81150A arbitrary waveform generator (AWG) while the detection was carried out by a 1.95mm diameter avalanche photodiode (APD) connected to an Agilent MSO71043 oscilloscope [15]. The post processing of the optical signal was done offline using a MATLAB script. More information regarding the APD receiver and the OFDM test configuration can be found elsewhere [15,16].

3. CW characteristics

The curves of optical power versus drive current for the standalone micro-LEDs of different sizes are plotted in Fig. 2(a). The slope is non-linear with the current and the curves eventually roll over at the highest currents. The smaller size micro-LEDs have a roll-over point at lower driving currents because they reach higher current densities for the same drive current. This non-linear behavior with the power roll over can be ascribed to an increase of the device temperature under operation, exacerbated by the phenomenon of efficiency droop [17,18]. The temperature rise can be related to the spectral shift of the peak emission illustrated in Fig. 2(b) in the case of the 100μm LED (black squares).
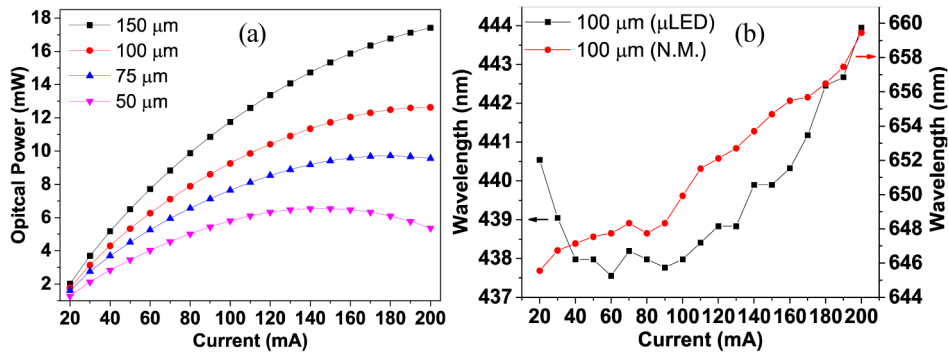
Fig. 2. a) L-I curve for each pixel in the μLED chip and b) spectral shift for the 100μm pixel and the III-V NM.

The emission from the micro-LED experiences an overall redshift of 3 nm, between 441 nm and 444 nm, between 20 mA and 200 mA. The LED peak emission wavelength starts blue-shifting at lower current before reaching a plateau (60 mA – 100 mA) and eventually red-shifting for current above 100 mA. The initial blue shift is attributed to band filling and carrier screening of piezoelectric fields in the active region. At higher current injection the reduction of the bandgap energy with temperature becomes the predominant effect, resulting in the red shift [19]. The device increase in temperature under bias current was verified through thermal imaging of the sapphire substrate of the micro-LEDs. It was found that the temperature surface of the sapphire increases by approximately 140°C between 20 and 200 mA due to self-heating. Self-heating in micro-LEDs has been previously studied [14].

Figure 3(a) plots the received optical power versus current for the hybrid micro-LEDs (650nm emission). We note that this measurement was performed with direct photodiode detection at the image plane of the set-up, without the use of an integrating sphere. The trend is similar, with the largest emitters giving the highest optical power, but the roll-over effect is more pronounced than for the stand alone micro-LEDs. For example, the 100μm stand-alone LED has a roll-over point between 180 and 200 mA whereas the equivalent hybrid LEDs roll over at 100 mA. At this current the forward power conversion efficiency (i.e. the measured power of the red hybrid LEDs divided by that of the standalone blue micro-LEDs) is close to 1.2%. The efficiency decreases continuously for higher current. This decrease is attributed to a reduction of the NM luminescence efficiency as its temperature increases, the NM being in contact with the sapphire substrate. The peak emission wavelength of this hybrid micro-LED as a function of the drive current is also plotted in Fig. 2(b) (red dots). Unlike the blue micro-LED emission, the spectrum continuously red-shifts, going from 645 nm at 20 mA up to 658 nm at 200 mA. The spectral emission of the AlInGaP NM is expected to redshift by approximately 0.12 nm/°C as determined from modeling based on the empirical Varshny relation [20]. Therefore the temperature increase of the NM can be inferred to be 100°C, which is not far off the temperature rise of the sapphire surface as measured by thermal imaging (140°C).
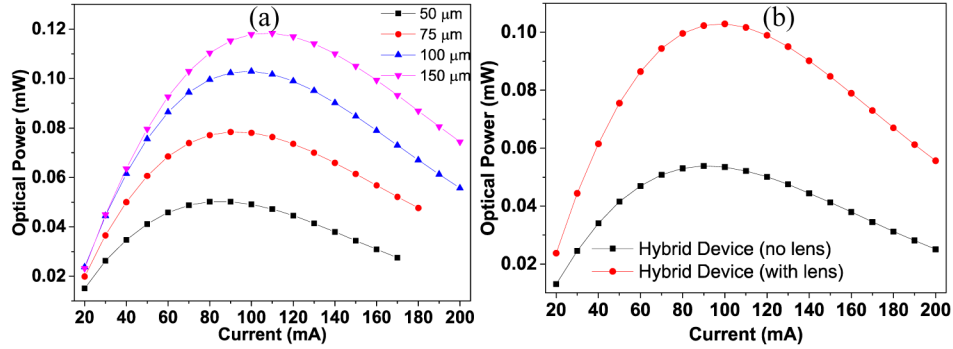
Fig. 3. a) L-I curve for the NM-hybrid devices and b) power enhancement by addition of the lens for the 100μm device.

The hemispherical lens added on top of the NM helps to increase the forward conversion efficiency as shown in Fig. 3(b) in the case of the 100μm device where the maximum output power doubles. The hemispherical lens mitigates the problem of waveguided light within the NM as well as increases the collection of photons close to the escape cone limit. It is found that the maximum output power is improved by 63%, 92%, 98% and 95% for the squared pixels with edge size of 150, 100, 75 and 50 μm, respectively. The lower enhancement for the 150μm device is probably because it sits on the edge of the lens. The addition of the lens however did not significantly improve heat removal from the NM; the red shift of the NM emission with current, with and without the lens, was found to be basically identical. For better thermal management, bigger lenses as well as active heat extraction from the lens could be used. Lenses could also be made with materials of higher thermal conductivity such as diamond.

In the description above, the decrease in the NM luminescence efficiency is attributed solely to a rise in temperature. Other possible explanations could include a dependence of non-radiative recombination on the MQW carrier density or a saturation of the NM absorption. To rule out these possibilities, the power density dependence of the converted light was further studied independently of the temperature rise caused by the micro-LED by remotely pumping a NM bonded onto a sapphire lens in the LD excitation configuration, as shown in Fig. 1(d). For low pump power density onto the NM, a micro-LED was used otherwise the LD was utilized. The spot size of the pump onto the NM surface, needed for determination of the pump power density, was measured using a beam profiler. Results plotted in Fig. 4 (black triangles) demonstrate that there is no saturation of the absorption and no noticeable increase in non-radiative recombination; the optical power from the NM increases linearly with the pump power density on a range of 0 up to 4 kW/cm^2. The left side of the broken x-axis are data under LED pumping whereas on the right side are data for LD pumping.

The converted power efficiency for this overall range is 0.88 ± 0.16%. The addition of a dielectric mirror, so that the NM is sandwiched between the lens and the mirror, increases the forward power efficiency to 1.14 ± 0.26% (red dots in Fig. 4), with an output power of 1.2 mW for a pump power density of 4 kW/cm^2.
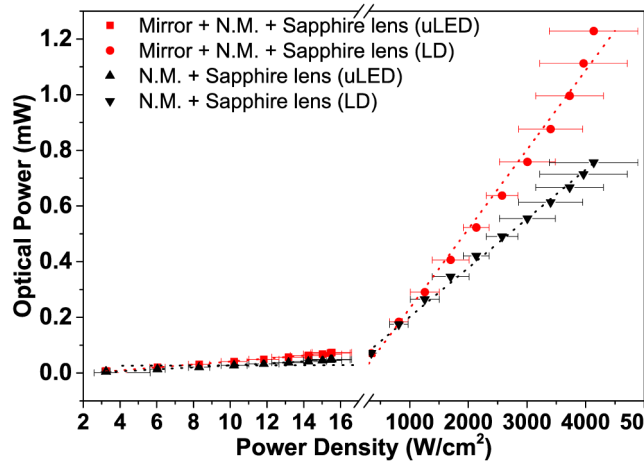
Fig. 4. Optical power vs power density for the NM bonded onto a sapphire lens and sandwiched between the sapphire lens and a dichroic mirror. Note break in the x-axis scale.

4. Dynamic characteristics

4.1 Bandwidth measurements

The optical modulation bandwidth (the frequency at which the modulated optical power is half the dc value) versus drive current for the different sizes of stand-alone and hybrid micro-LEDs are plotted in Fig. 5(a) and 5(b) respectively. The intrinsic bandwidth of NM is plotted in Fig. 5(c).
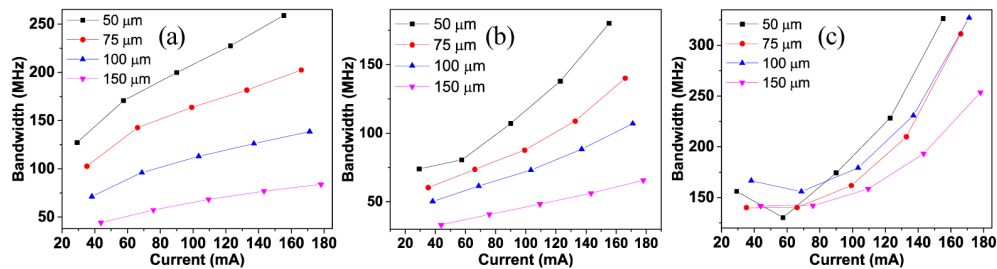
Fig. 5. Bandwidths for a) the stand-alone micro-LEDs b) the hybrid micro-LEDs and c) the NM, extracted from a) and c) as explained in [9].

The bandwidth is size- and current-dependent reaching a maximum of 260 MHz and 180 MHz at around 150 mA for the standalone micro-LED and the hybrid red device, respectively. The current dependence can be attributed to the reduced carrier lifetime in the active region of the micro-LEDs as the current, and hence the carrier density, increases [12,21]. The response of the NM, obtained by subtracting the standalone micro-LED response to the response of the hybrid device [9], further affects the bandwidth of the hybrid sources. The intrinsic response of the NM is between 130 MHz and 320 MHz, which is at least two order of magnitude faster than conventional phosphors [22]. The increase in the bandwidth with the current is linked to the increase of non-radiative recombination as the temperature of the device, hence of the NM, increases.

The frequency response of the LD could not be measured, as it was higher than the photodiode bandwidth of 1.4 GHz [23,24]. However, the laser excited bandwidth of the NM bonded onto the sapphire lens bandwidth was measured and is shown in Fig. 6.
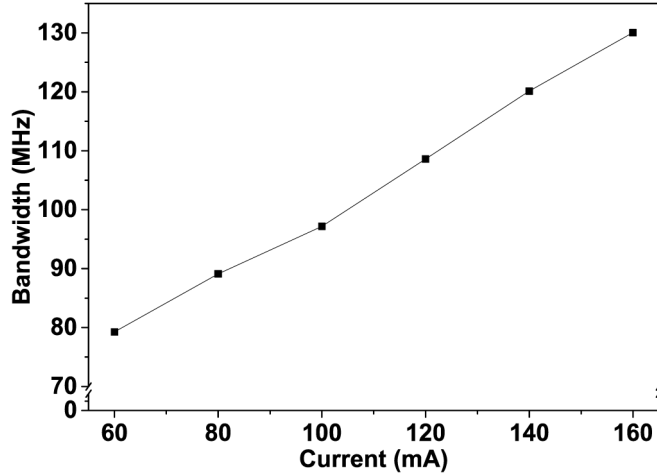
Fig. 6. Bandwidth from the LD-pumped NM-lens structure (the line is a guide to the eye).

In Fig. 6 the bandwidth is set by the intrinsic response of the NM. There is a difference between the maximum achievable bandwidth, 180 MHz for the hybrid device and 130 MHz for the LD-pumped NM. Again, this is due to the increase of non-radiative recombination caused by heating when the NM is integrated onto the micro-LED array. When remotely-pumped the heating in the NM is nowhere near as severe.

4.2 M-PAM measurements

Free-space optical data transmission, using the NM device formats described above, was carried out. The optical set-up and the required equipment were described in section 2.2. A pseudo random binary sequence (PRBS) of 10^{14}-1 was generated and encoded into appropriate PAM level, which was then loaded to the Agilent 81180A AWG. A fractionally-spaced adaptive decision feedback equalizer (DFE) was adopted at the receiver.

The BER vs. data rates for PAM scheme for the hybrid micro-LEDs are presented in Fig. 7 and the achieved data rates at BER of 3.8 x10^{-3} are summarized in Table 1. The smallest micro-LED offered the highest data rate for all modulation schemes due to its higher bandwidth. Among PAM schemes, 4-PAM with DFE offered the best performance closely followed by 2-PAM. These results follow the theoretical predictions in [25] and experimental results in [26]. It is theoretical shown in [26] that 4-PAM with DFE requires less optical power than 2-PAM with DFE when data rate is beyond 5-times the electrical bandwidth. Higher level PAM has higher power penalty due to LED and device non-linearity. Hence, non-linearity compensation is required for improved performance. The non-linearity compensation is, however, not within the scope of this paper.

Table 1. Achievable data rates at BER of 3.8 × 10^{-3} for the different size of hybrid micro-LEDs in Mbit/s.

	50 x 50 μm^2	75 x 75 μm^2	100 x 100 μm^2	150 x 150 μm^2
2-PAM	777	757	738	659
4-PAM	867	862	807	615
8-PAM	720	740	680	495
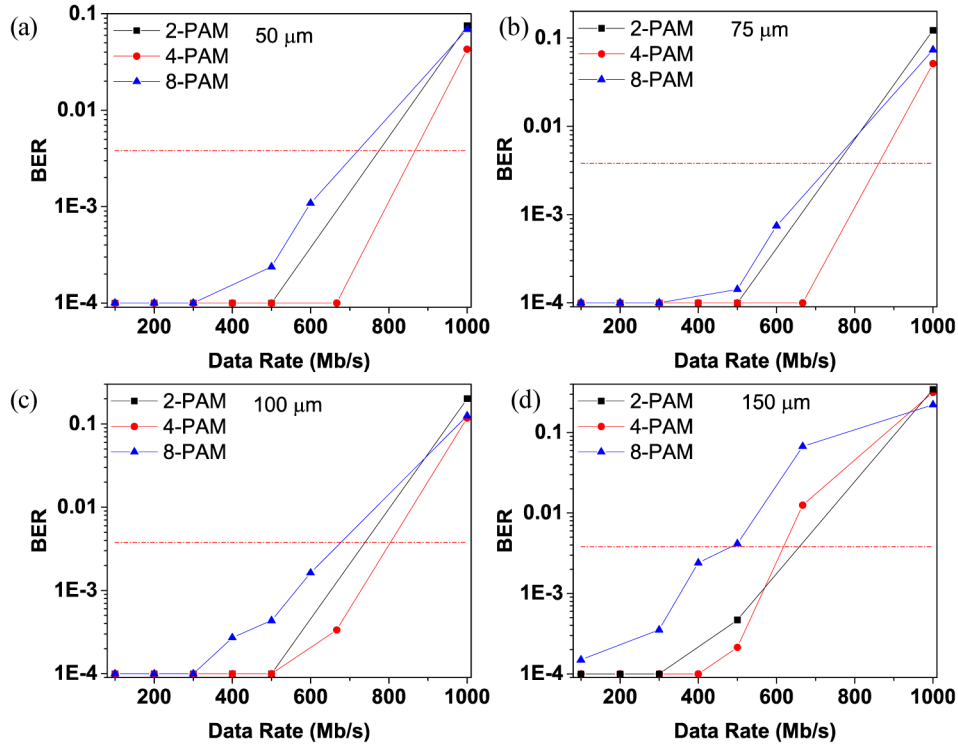
Fig. 7. BER vs Data Rate for the hybrid devices a) 50μm x 50μm pixels, b) 75μm x 75μm pixels, c) 100 μm x 100μm pixels and d) 150μm x 150 μm pixels.

DCO-OFDM data transmission using the LD-pumped NM [Fig. 1(d)] was also tested. By adjusting the LD driving bias current and the modulation depth, it was possible to achieve transmission up to 1.2 Gb/s at BER of 3.8×10^{-3} as shown in Fig. 8. The higher data rate is due to the combined higher SNR level and higher modulation bandwidth of the laser diode in comparison to the micro-LEDs.
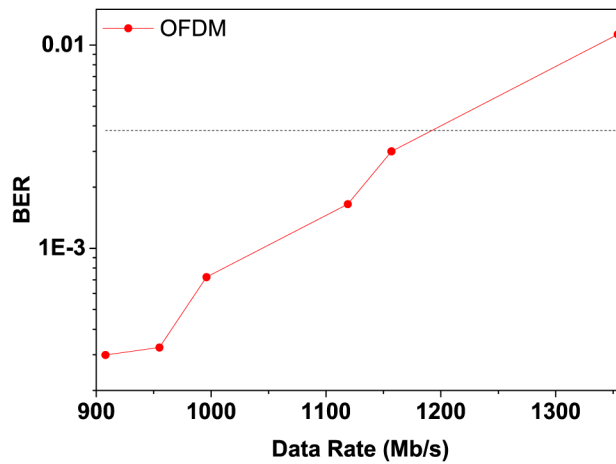

Fig. 8. BER vs Data Rate for the sample pumped with a laser diode.

5. Conclusion

In this paper, we have demonstrated VLC using InGaN sources color-converted with AlInGaP NM assemblies. The NM geometry of the converter enables integration with optics and micro-LEDs by capillary bonding. We note that this format of color-conversion is consistent with semiconductor approaches developed by some LED manufacturers in order to extent the efficiency of blue LEDs to longer wavelengths, while at the same time offering faster response than phosphors for VLC. The extraction efficiency values reported are still relatively low but could be improved by further incorporating light extraction features to the NM assembly. The maximum data rate achieved for this hybrid configuration in this paper was 870 Mb/s using 4-PAM scheme with DFE. We also reported on a NM format for remote pumping by LD. In this configuration we have shown VLC up to 1.2 Gb/s using OFDM. This second configuration would be particularly suited for high power applications with the NM bonded to optics and heat spreaders. Finally, by designing other NM structures using AlGaInP or InGaN material systems it should be possible in principle to extend the wavelength coverage across the visible spectrum.